

Enhanced *In Situ* Spatial Proteomics by Effective Combination of MALDI Imaging and LC-MS/MS

Authors

Frederike Schäfer, Archana Tomar, Shogo Sato, Raffaele Teperino, Axel Imhof, and Shibojyoti Lahiri

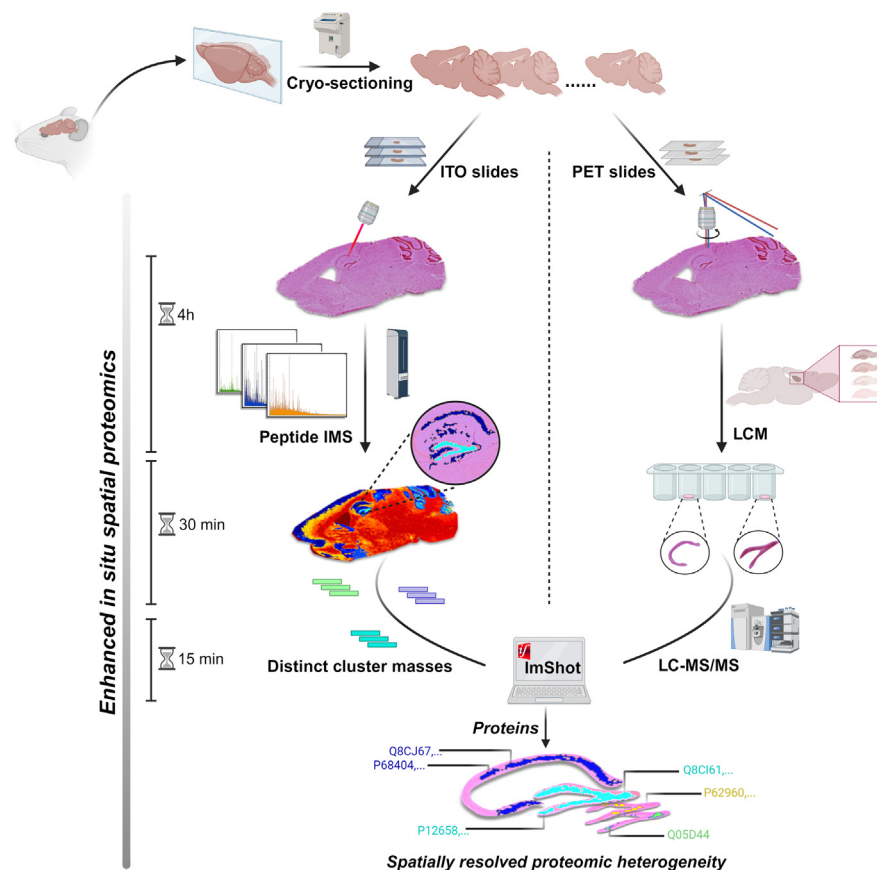
Correspondence

imhof@lmu.de; shibojyoti.lahiri@med.uni-muenchen.de

In Brief

This study integrates MALDI-IMS with laser capture microdissection (LCM) coupled to LC-MS/MS to achieve simultaneous detection of multiple proteins at near-single-cell resolution. By leveraging MALDI-IMS's spatial resolution and LCM-LC-MS/MS's deep regional proteomic coverage, we precisely annotate and localize proteins within the mouse hippocampus. This approach reveals distinct protein compositions, that are validated by spatial transcriptomics and data mining. Our method is high-throughput, cost- and time-effective, providing significant advancement for detailed investigations into cellular heterogeneity and molecular underpinnings of diseases.




Graphical Abstract



Highlights

- Novel, systematic combination of cutting-edge technologies for *in situ* proteomics.
- Combining spatial proteomics, transcriptomics, and data mining for validation.
- Pipeline shows cellular proteomic signatures and local differences in the dentate gyrus.
- Rapid, cost-effective method with widespread applicability in biomedical research.

Enhanced *In Situ* Spatial Proteomics by Effective Combination of MALDI Imaging and LC-MS/MS

Frederike Schäfer^{1,2,3,4}, Archana Tomar^{3,4}, Shogo Sato⁵ , Raffaele Teperino^{3,4}, Axel Imhof^{1,2,*} , and Shibojyoti Lahiri^{1,2,*} 

Highly specialized cells are fundamental for the proper functioning of complex organs. Variations in cell-type-specific gene expression and protein composition have been linked to a variety of diseases. Investigation of the distinctive molecular makeup of these cells within tissues is therefore critical in biomedical research. Although several technologies have emerged as valuable tools to address this cellular heterogeneity, most workflows lack sufficient *in situ* resolution and are associated with high costs and extremely long analysis times. Here, we present a combination of experimental and computational approaches that allows a more comprehensive investigation of molecular heterogeneity within tissues than by either shotgun LC-MS/MS or MALDI imaging alone. We applied our pipeline to the mouse brain, which contains a wide variety of cell types that not only perform unique functions but also exhibit varying sensitivities to insults. We explored the distinct neuronal populations within the hippocampus, a brain region crucial for learning and memory that is involved in various neurological disorders. As an example, we identified the groups of proteins distinguishing the neuronal populations of the dentate gyrus (DG) and the cornu ammonis (CA) in the same brain section. Most of the annotated proteins matched the regional enrichment of their transcripts, thereby validating the method. As the method is highly reproducible, the identification of individual masses through the combination of MALDI-IMS and LC-MS/MS methods can be used for the much faster and more precise interpretation of MALDI-IMS measurements only. This greatly speeds up spatial proteomic analyses and allows the detection of local protein variations within the same population of cells. The method's general applicability has the potential to be used to investigate different biological conditions and tissues and a much higher throughput than other techniques making it a promising approach for clinical routine applications.

Individual cells within a tissue differ in morphology and function by differences in their molecular makeup. Variations in regional protein composition have been described in a variety of organs like the brain (1–3), heart (4–6), liver (7–9), and kidney (10–12), and loss of cellular heterogeneity and function has been associated with many different diseases (8, 10, 13–15). In recent years, remarkable progress has been made in molecularly describing single cells thereby generating a better understanding of cellular heterogeneity and identity (16–19). However, most single-cell analyses were made in disintegrated tissues resulting in a lack of contextuality, thereby limiting the knowledge gained by these methods. Further, investigation of molecular variations across and within different cell types is particularly important in intact tissues, where both the diagnostic and prognostic information of diseases are intact.

Although approaches to address this issue have been developed particularly on the transcriptomic level (17, 20–23), commercially available options have not yet reached single-cell resolution *in situ*. Implementing approaches to analyze spatial protein composition on a proteome-wide level has proven to be considerably more challenging due to the minimal input material generated by a single cell. In addition, these workflows are associated with very low cost efficiency and high overall analysis time making them practically inconvenient for a routine application of spatial proteomics analysis (18, 24–27). A much faster technique where spatial information of the proteome is maintained is MALDI Imaging mass spectrometry (MALDI-IMS). Here, analyte composition is determined *in situ* by laser-induced ablation of a matrix-coated tissue, thereby generating a mass spectrum for each defined pixel on the tissue (28). The protein composition for every position on the tissue can therefore be determined,

From the ¹Faculty of Medicine, Department of Molecular Biology, and ²Protein Analysis Unit, Faculty of Medicine, Biomedical Center Munich, Ludwig-Maximilians Universität München, Munich, Germany; ³Institute for Experimental Genetics, Helmholtz Zentrum München, German Research Center for Environmental Health, Munich, Germany; ⁴Environmental Epigenetics Group, German Center for Diabetes Research (DZD), Munich, Germany; ⁵Center for Biological Clocks Research, Department of Biology, Texas A&M University, College Station, Texas, USA
*For correspondence: Axel Imhof, imhof@lmu.de; Shibojyoti Lahiri, shibojyoti.lahiri@med.uni-muenchen.de.

subsequently allowing unbiased clustering of local spectra by similarity. By comparing such clusters to histological staining of the same tissue, molecular signatures of specific cell types *in situ* may be determined. However, direct, resource-independent, and high-throughput identification at the proteomic level is still not achievable. Here, we demonstrate a combination of experimental and data integration pipelines that allow the investigation of both local and global proteomic distinction in different cell types. We choose the mouse brain as a representative tissue, where a multitude of different cell types not only fulfill very distinct functions in the brain but also vary in their sensitivity to insults, be it genetic or environmental (2, 29–32).

In this report, we focus on the hippocampal region of the mouse brain and study the proteomic variations both across and within the two distinct neuronal populations of the dentate gyrus (DG) and the cornu ammonis (CA). The hippocampus is of particular interest due to its central role in learning and memory and its involvement in many neurological disorders (33–37). Unbiased hierarchical clustering of MALDI-IMS data was employed to identify cellular subpopulations characterized by distinct peptide compositions. The characteristic proteomic makeup of these cells was determined using the in-house developed software ImShot, which employs most likely peptide (MLP) scoring (38). This was achieved by matching the peptides to their respective parent proteins derived from LC-MS/MS analysis of corresponding laser capture microdissected (LCM) brain regions. Our analysis could indeed distinguish the two neuronal populations proteomically. In addition to observed cell-type-specific enrichment being confirmed by public data, regional enrichment of identified proteins overlapped with their respective transcripts. We could also reveal local protein differences within the granule cell layer of the DG. While protein profiles are largely consistent across different animals, the variations depend on the individual animal, the specific brain coordinates examined, and the genotype. The fact that, once the masses have been identified using ImShot, the comparison of the different conditions can be performed on MALDI-IMS measurements only makes the spatial proteomics approach much less time-intensive and more cost-effective than others previously described (39). The general applicability of the method allows it to be used as a fast and reliable method to get precise and spatially resolved proteomic information from different regions of the same tissue section.

EXPERIMENTAL PROCEDURES

Animals

Brains of age-matched male wild-type C57BL/6J and Cryptochrome 1/2 double knockout (*Cry1/2^{-/-}*) (40) were obtained from the lab of the late Paolo Sassone-Corsi at the University of California, Irvine (UCI), California, USA. Mice were fed a standard rodent laboratory diet *ad libitum* and reared at 24–25 °C on a 12-h light/dark cycle.

Animal handling was in accordance with guidelines for the use of animals for research purposes. Animals were maintained at the UCI animal facilities. Animal experiments were approved by the Institutional Animal Care and Use Committee (IACUC) of UCI (AUP-18–022). Mice were sacrificed at 6 months to isolate brains. Brains were snap-frozen in liquid nitrogen and shipped on dry ice. Upon arrival, brains were stored at –80 °C until usage.

Experimental Design and Statistical Rationale

MALDI Imaging Mass Spectrometry was performed on 5 mice brains across 2 genotypes (three wildtype (WT) brain tissues and two *Cryptochrome 1/2* double knock-out (*Cry1/2^{-/-}*). Representative and preferential spatial distribution of peptides could be ensured thus. For deep proteome analysis, proteins were extracted from 4 biological replicates (two biological replicates were used per genotype). In the laser capture microdissection (LCM), hippocampal populations of dentate gyrus granule cells and CA pyramidal cells were excised from 10 technical replicates for each brain to extract proteins and subsequently generate peptides from them. Due to the highly selective excision of target cell populations and pooling over multiple sections, we expect minimal variation between replicates.

For the analysis of acquired IMS data, hierarchical clustering was performed for cluster identification. Here, pixel-based statistical analysis was used to assign groups based on spectral similarity (41). Discriminative masses between clusters were identified using receiver operating characteristic (ROC) curve analysis to ascertain the discriminatory power of individual *m/z* values. Only *m/z* values considered to be highly discriminative (0.7–0.9) were included in the downstream analysis. In the case of LC-MS/MS data, LIMMA (linear models for microarray data) statistical testing was employed for statistical comparison of protein abundances between the DG and CA from all the animals. This uses the whole dataset to shrink the estimated sample variances of each protein towards a pooled estimate.

MALDI-Imaging Mass Spectrometry

Sample Preparation—Mouse brains of 3 age-matched WT and 2 *Cry1/2^{-/-}* were halved mid-sagittally and sectioned on a Leica CM3000 cryostat (Leica Biosystems). 12- μ m sections were thaw-mounted onto indium-tin-oxide (ITO) coated glass slides (Bruker Daltonics GmbH) coated with polyL-Lysine (1:1 in water, 0.1% NP40). Sections were stored in a sealed container at –80 °C until usage.

Before digestion and matrix application, sections were washed according to a pre-established protocol to remove interfering salts and lipids (42). In brief, proteins were precipitated *in situ* by incubating in 70% Ethanol and 100% Ethanol for 30 s each, followed by 2 min incubation in Carnoy's fluid (60% EtOH, 30% chloroform, 10% acetic acid (v/v/v)) and acidification in 0.1% TFA, the excess of which was subsequently neutralized by 20 mM ammonium bicarbonate. The slides were dried under vacuum overnight at room temperature.

For *in situ* protein digestion, sections were sprayed with 0.025 mg/ml trypsin (Sigma-Aldrich) in 20 mM ammonium bicarbonate using the HTX TM Sprayer (HTX Imaging, HTX Technologies) following the manufacturer's method. Samples were then immediately incubated at 50 °C in humid conditions for 2.5 h. After tryptic digestion, sections were sprayed with matrix (10 mg/ml α -Cyano-4-hydroxycinnamic acid (HCCA) in 70% ACN; 1% TFA) using an HTX TM Sprayer (HTX Imaging, HTX Technologies) with the standard manufacturer's method.

IMS Measurement—Peptide measurements from 5 mouse brain tissues were carried out using a rapifleX MALDI tissue-typer MALDI-TOF/TOF mass spectrometer (Bruker Daltonics GmbH). Samples were measured at 20 μ m spatial resolution and within a mass range of 500 to 3200 *m/z* using positive reflector mode. For calibration prior to measurement, a peptide calibrant solution (Peptide calibration

standard II, Bruker Daltonics GmbH) was spotted at different positions on the same slide.

After IMS measurements, the HCCA matrix was removed with 70% EtOH, and the tissue was stained with hematoxylin and eosin (HE). High-resolution images of the sections were generated using the Leica THUNDER Imager 3D Live Cell TIRF (Leica Biosystems) in brightfield mode and an HC PL APO 20x/0.80 objective. The generated images were co-registered to IMS data to allow histological correlation.

Data Analysis

IMS data were further calibrated by post-acquisition statistical calibration in flexAnalysis (Bruker Daltonics GmbH) and imported into SCiLS Lab 2016b (Bruker Daltonics, www.scils.de) for further analysis. The unsupervised automated segmentation pipeline was used on calibrated and total ion count normalized data with a minimum interval width of 0.1 Da for hierarchical clustering, where similar spectra were grouped into the same colored, expandable clusters. This method uses statistical analysis to group similar spectra from a given region into a single cluster. All spectra from a certain cluster are then assigned a color and shown as label maps, with all pixels color-coded based on their cluster assignment. We have used bottom-up hierarchical clustering to successively group the most similar spectra by using correlation distance metric and average linkage (41). Clusters representing regions of interest as well as sub-regional clusters were annotated. Distinguishing masses between clusters were identified using the "Find discriminative m/z values" tool which is based on a ROC analysis. Here, a ROC curve based on the m/z values estimated sensitivity and specificity is plotted. Area under the curve values between 1 and 0 describe the discriminatory power of each m/z value. Thresholds between 0.9 and 0.7 were used for inter- and intraregional comparisons respectively (Supplemental Files S1–S5). The resulting mass lists were exported for deisotoping (Supplemental Files S6–S10) and protein identification by correlation with LC-MS/MS data by ImShot (38).

LC-MS/MS

Laser Capture Microdissection—Four mouse brains (two biological replicates of each WT and *Cry1/2^{-/-}* animals) were sectioned into 50 μm sagittal sections and mounted onto metalframe PET slides (Leica Biosystems). The sections were stained with Nissl staining (43) to visualize brain regions for LCM. A Leica LMD 7000 with a 5x objective was used for LCM. The laser setup was configured as follows: Pulse frequency - 120, maximum pulse energy - 50, aperture - 17, Speed - 10, Head current - 100%, Offset - 65. Regions of interest were manually selected and tissue of 10 technical replicates per biological replicate was pooled. From each brain section, the neuronal populations of the hippocampus, namely dentate gyrus granule cells (DG) as well as pyramidal cells of CA were dissected for further analysis.

Sample Preparation—Laser-microdissected samples were processed using the PreOmics iST Kit for mammalian tissue according to the manufacturer's guide (PreOmics GmbH, Martinsried Germany). To enhance tissue lysis, lysis buffer was added, and sections were homogenized manually using Micro-homogenizers, PP (Carl Roth GmbH+Co. KG) before sonication. The lysate was then incubated with trypsin/LysC digestion solution for 3 h at 37 °C for protein digestion. The resulting peptides were desalted, purified, and subsequently dried in a speed vac, followed by resuspension in 10 μl "LC LOAD" buffer for LC-MS/MS measurement.

Mass Spectrometry

For reversed phase HPLC separation of peptides on an Ultimate 3000 nanoLC system (Thermo Fisher Scientific), 5 μl of the solution

was loaded onto a 15 cm analytical column (75 μm ID with ReproSil-Pur C18-AQ 2.4 μm from Dr Maisch), washed for 5 min at 300 nl/min with 3% ACN containing 0.1% FA and subsequently separated applying a linear gradient from 3% ACN to 40% ACN over 50 min. Eluting peptides were ionized and detected on a QExactive HF mass spectrometer (Thermo Fisher Scientific). The mass spectrometer was operated in a TOP10 method in positive ionization mode, detecting eluting peptide ions in the m/z range from 375 to 1600. Peptide ion masses were acquired at a resolution of 60,000 at m/z 400 (AGC target of 3×10^6) while MS/MS spectra were acquired at a resolution of 15,000 at 400 m/z (AGC target of 1×10^5 , ion selection threshold 3.3×10^4). All MS1 mass spectra were internally calibrated to lock masses from ambient siloxanes. Precursors were selected based on their intensity from all signals with a charge state from 2+ to 5+, isolated in a 2 m/z window, and fragmented using a normalized collision energy of 27%. To prevent repeated fragmentation of the same peptide ion, dynamic exclusion was set to 20 s.

Data Analysis

Identification was carried out using MaxQuant (44) v2.1.0.0. Default MaxQuant conditions were used with parent and fragment ion mass tolerances of 20 ppm. The allowance of missed cleavages was set to 2. For the searches, the reviewed mouse canonical protein database from Uniprot (release date 01.12.2020; 34,336 entries) was used. Additionally, the following conditions were used: protein FDR and peptide FDR of 0.05 and 0.01, respectively; minimum peptide length of 5; variable modifications of oxidation (M), acetyl (protein N-term), acetyl (K), methyl (KR) and dimethyl (KR)); fixed modification of carbamidomethyl (C); peptides for protein quantification, razor and unique; minimum peptides of 2; minimum ratio count of 2. Protein validation was carried out based on a unique peptide detected in all or at least 50% of the replicates.

Statistical Analysis—The in-house developed software ImShot (38, 45) was used for LIMMA statistical analysis. MaxQuant-generated peptide.txt and protein.txt files were used as input for comparison of DG and CA. Missing values were imputed using "tiny" imputation and normalization was set to column-wise. K out of N was set to 1, sequence coverage to 5%, and unique peptides to 1 (Supplemental Files S11 and S12). Proteins that were detected in only one group were considered to be exclusive for that group and were excluded from further statistical analysis.

Data Integration and Analysis—Data integration was carried out using output from differential analysis of LC-MS/MS data and deisotoped IMS clustered mass lists. Tolerance for IMS measurement and MLP scoring was set between 0.2 Da - 0.3 Da and 0.15 Da - 0.2 Da, respectively (Supplemental Files S13–S17). MLP (Most Likely Peptide) scoring was calculated based on the mean intensity of a peptide (μ), the moderated *p*-value of the same peptide (p_{mod}) and the \log_2 fold change between two groups ($\log_2\text{FC}$) according to the following equation: $\text{MLP} = (\mu \cdot \log_2(\text{FC}) / p_{\text{mod}})$.

Cellular localization of identified proteins was determined using the Uniprot database (Supplemental File S18).

Validation of Protein Localization Using Data Mining

Localizations and enrichments of identified proteins from each cluster were validated using the Mouse Genome Informatics database (MGI, <https://www.informatics.jax.org/tools.shtml>) and the Allen Brain Atlas data portal (<https://mouse.brain-map.org/search/index>) (46). MGI gene expression data was searched by first navigating to the "Gene expression database" (<https://www.informatics.jax.org/gxd/>), where a list of genes was uploaded. Next, we selected the hippocampal formation as our anatomical structure of interest, followed by the search function. Using the "Tissue x Gene Matrix" tab, we filtered for the dentate gyrus and hippocampus CA. *In situ* hybridization (ISH)

data deposited in Allen Brain Atlas was searched by using the “Gene search” (46–52).

Spatial Transcriptomics

Spatial transcriptomics was investigated using the 10× Visium Spatial Gene Expression platform (10× Genomics). Sagittally cut brain halves were scored to 6.5 mm × 6.5 mm and 10 μm sections were cut using Leica CM3000 cryostat (Leica Biosystems). Sections were thaw-mounted onto fiducial frames of Visium Spatial Gene Expression slides and stored at –80 °C for <1 week. Samples were processed according to the manufacturer’s guide. In brief, the tissues were stained with hematoxylin and eosin and imaged on a Leica THUNDER Imager 3D Live Cell TIRF (Leica Biosystems) in brightfield mode and a N PLAN 5×/0.12 PHO 11506303 objective. Tissues were then permeabilized for 30 min at 37 °C to release mRNA onto slide-bound probes, followed by cDNA synthesis, amplification, and quantification. Quantification and quality control were carried out using the DNA High Sensitivity Kit of the TapeStation (Agilent). Subsequently, a sequencing library was constructed, and quality was controlled by the DNA High Sensitivity Kit of the TapeStation (Agilent), followed by post-library construction quantification by the KAPA Library Quantification Kit for Illumina platforms. Libraries were sequenced on an Illumina NovaSeq 6000 (SP-100 flow cell, 138 bp reads, 2 lanes). Read mapping, differential gene expression analysis, and visualization were carried out with the Space Ranger pipeline and Loupe Browser software provided by 10× Genomics (Supplemental File S19).

RESULTS

Comprehensive Detection of Spatially Resolved Proteome Signatures in the Brain

By combining MALDI-IMS with laser capture microdissection and a spatial gene expression analysis (Fig. 1A), we could generate a highly multiplexed and exhaustive view of the brain at a molecular level. Sagittal mouse brain sections were imaged at a pixel size of 20 μm. This spatial resolution allowed us to annotate several regions, which are characterized by distinct proteomic signatures (Fig. 1B). In the hippocampus, the two different neuronal populations of CA1 pyramidal cells and the DG granule cell layer could be separated. Similarly, separate clusters within the cerebellum characterized the known layers of white matter (WM), granule cell layer (CB GCL), purkinje cell layer (CB PCL), and molecular layer (CB ML) (Fig. 1B). To assign the most probable identities to the distinct proteins for each hippocampal cluster (brain region) and distinguish potential sub-clusters, defined regions of the hippocampus were excised by LCM and profiled by high-resolution shotgun proteomics (Fig. 1C). We identified between 4500 and 5000 proteins for each of the dissected regions (Fig. 1C). The PCA plots for MALDI-IMS and shotgun proteomics consistently show the segregation of the datasets into distinct brain regions, indicating that the *in situ* peptide signatures (Fig. 1D, left panel) as well as LCM-LC-MS/MS identification (Fig. 1D, right panel) allows a distinction of the different regions within a single section.

Analysis of the Hippocampus Reveals Region-Specific Peptide Signatures that Correlate with Cellular Localization of the Parent Proteins

Histological correlation of the acquired IMS data showed clear and distinct peptide signatures (Fig. 2A) that could consistently distinguish the granule cell population of the hippocampus along with another major region, the CA 1 (Fig. 2B and Supplemental Figs. S1 and S2).

Profiling of DG and CA1 by LCM-LC-MS/MS revealed enrichment of 1601 and 1874 proteins in the respective neuronal populations (Supplemental File S12). Using our in-house developed software ImShot to assign identities to the MALDI-IMS peptides (38), we considered the peptides discriminating DG from CA1 and vice-versa. On average, we could annotate around 40 proteins for DG and CA1 each across all 5 animals analyzed (Fig. 2C). Importantly, most of the assigned proteins distinguishing the DG cluster from CA1 were of nuclear origin, while CA1-enriched proteins were predominantly cytosolic (Fig. 2D). As the density of nuclei within the DG is higher than that in the CA1, our method lends credence to the *in situ* identifications by correlating well with the morphological characteristics of the two hippocampal regions. Considering the ‘Nucleus’ fraction of the pie charts in Figure 2D, we observe that the relative distribution of nuclear proteins within the DG and CA is independent of the genotypes analyzed.

Distinct Peptide Clusters Define DG and CA1 Regions with Consistent Enrichment Patterns

Representative distribution patterns of the clusters (collection of multiple proteins) defining the DG and CA1 regions are displayed in Figure 3A. Investigating animals from 2 different genotypes (WT and *Cry1/2^{-/-}*) allowed us to select region-specific proteins that are independent of animal genotype and hence appropriate readouts for experimental reproducibility. Upon further breakdown of these clusters into individual peptides/proteins, we see a consistent enrichment of these in their respective regions. Among others, gene products of *Calb1*, *Bag4*, and *Ptma* were found to be discriminative for DG, while *Prkcb*, *Stau2*, and *Idh3g* represent CA1. These proteins show clear enrichment in their respective region (Fig. 3A right top panel, Fig. 3B for DG and Fig. 3A right bottom panel, and Fig. 3C for CA1; Supplemental Fig. S3). Once identified as discriminative, these proteins were observed to be consistently enriched in their respective regions regardless of the genotype (Fig. 3, B and C and Supplemental Fig. S4).

Spatial Transcriptomic Analysis and Data Mining Corroborates In Situ Protein Annotations

Using spatial transcriptomics at 50 μm spatial resolution, we looked at the distribution of the transcripts that encode the discriminating proteins of DG and CA identified *in situ*.

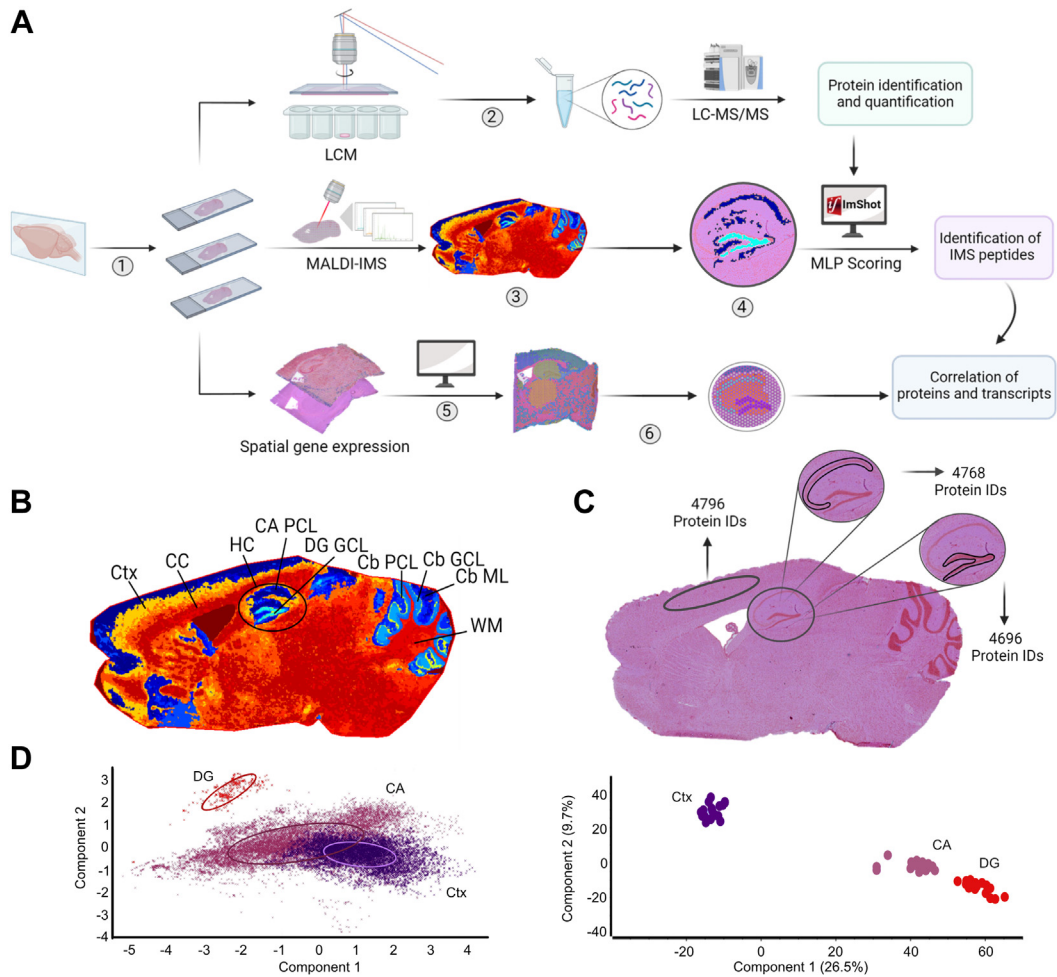


FIG. 1. Combining high-resolution MALDI-IMS with regional LC-MS/MS and spatial transcriptomics. **A**, (1) C57BL/6J mouse brains were sagittally halved and cut into serial sections (2). Dentate gyrus granule cell layer (DG) and cornu ammonis pyramidal cell layer (CA1) were excised by laser capture microdissection and protein extraction was performed, followed by LC-MS/MS measurement and protein identification and quantification (3). In parallel, MALDI-IMS peptide measurement was carried out on serial sections (4). Hierarchical clustering according to spectral similarity across the whole tissue was performed and discriminative masses determined. The resulting clustered mass lists as well as LC-MS/MS results were used as input for ‘MLP scoring’ and identification of IMS peptides using the software ImShot (5). Additionally, spatial gene expression analysis was performed and data was clustered according to transcriptomic similarity (6). Enrichment analysis was performed on manually annotated regions of interest and results were correlated to spatial proteome. **B**, representative image of IMS data after hierarchical clustering. Brain regions can be characterized based on local peptide signatures. **C**, hematoxylin-eosin (HE) staining of the same sagittal mouse brain section. Highlighted areas were excised by laser capture microdissection. **D**, PCA plots of IMS data with 50% error ellipses (*left*) and LCM-LC-MS/MS data (*right*). Ctx, Cerebral cortex; CC, Corpus callosum; CA PCL, Cornu ammonis pyramidal cell layer; Cb PCL, Cerebellar purkinje cell layer; Cb GCL, Cerebellar granule cell layer; Cb ML, Cerebellar molecular layer; DG GCL, Dentate gyrus granule cell layer; HC, Hippocampus; WM, White matter.

Statistical analysis of LCM-LC-MS/MS data revealed an enrichment of 1601 proteins in the DG as compared to CA. Of those, ~55% (a total of 880), also displayed differences at the transcript level. A comparison of MLP-identified proteins revealed that a similar fraction of discriminative proteins is also different at the transcript level in CA and DG (Fig. 4A). Quantification of the representative distribution patterns of the transcripts coding for enriched proteins in the proteomic analysis (Fig. 3) validates their respective regional enrichment (Fig. 4B). Transcripts of Bag4, Ptma, and Calb1 show higher expression in DG while those of Prkcb, Stau2, and Idh3g are

enriched in CA, thereby matching our observations on the protein level. Further validation was conducted *in silico* by mining publicly available data deposited in the Allen Brain Atlas (46). Clear enrichment of Bag4 and Calb1 can be observed in the DG, while Ptma displays comparative expression levels in DG and CA. Due to the lack of quantification numeric, precise differences cannot be computed and matched to our results in this specific case. Gene products of Prkcb, Stau2, and Idh3g are highly enriched in CA as compared to DG, corroborating our findings on both transcript and protein levels.

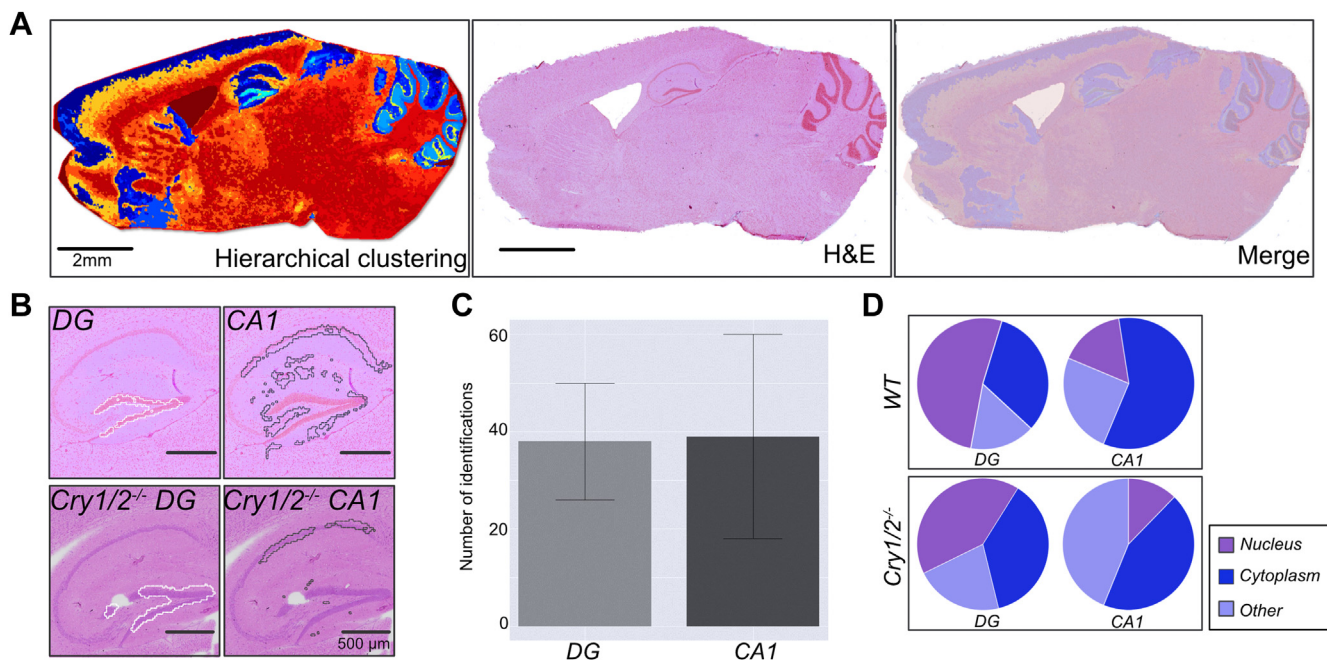


FIG. 2. MALDI-IMS reveals hippocampal tissue morphology-related distinct peptide clusters. **A**, comparison of MALDI-IMS peptide data after hierarchical clustering (Left panel) and hematoxylin-eosin staining (Middle panel) for morphological correlation (Right panel). **B**, outline of generated peptide clusters within the hippocampus in WT (Top panel) and *Cry1/2^{-/-}* (Bottom panel). A distinct cluster characterizes the dentate gyrus granule cell layer (DG, Top left) of WT animals, while the cluster of cornu ammonis pyramidal layer includes additional areas (CA1, Top right). Similar, but more defined patterns are observed for the *Cry1/2^{-/-}* animals (Bottom left and right). **C**, the average number of assigned proteins by MLP scoring in DG and CA1. **D**, correlation of MLP-identified discriminative proteins to their cellular localization based on comparison of DG vs CA1 in WT (Upper panel) and *Cry1/2^{-/-}* (Bottom panel).

Local Variations in Protein Abundance Across the Dentate Gyrus

Successful validation of protein annotations generated by our pipeline allowed us to investigate further the proteomic characteristics of the highly distinctive region of DG. Upon closer inspection, we observed that many peptides display local variations in their distribution across the DG. Importantly, similar patterns of variation were observed across multiple peptides, allowing for groupwise assessment of local proteomic heterogeneity (Fig. 5A). Two distinct groups of peptides having different distribution patterns (LV1 and LV2) were found to be enriched in DG. Groups representative of these distinct variation patterns allowed our pipeline to assign the respective parent proteins. This enabled us to increase the depth of our coverage further as the number of annotated proteins increased from 38 to 58 within the DG (Fig. 5B). The local enrichment of these proteins within the DG was validated by publicly available gene expression data deposited in the Mouse Genome Informatics (MGI) database (Fig. 5C).

Expectedly, the regional variations showed different degrees of consistency across the animals. Groups of proteins having similar distribution patterns like *Ybx1* or *Eif5b* are enriched in the DG across all animals (Fig. 5, D and E and Supplemental Files S13–S17). However, the distribution and enrichment of some proteins, although distinct for DG, show

different distribution patterns between animals and areas of sectioning (Supplemental Files S13–S17).

DISCUSSION

The advancement of technology in biomedical research has significantly enhanced our understanding of cellular heterogeneity within tissues. This study showcases the potential of integrating MALDI-IMS with LCM-LC-MS/MS to achieve near-single-cell resolution in spatial proteomics. The combination of MALDI-IMS and LC-MS/MS leverages the strengths of both techniques. MALDI-IMS provides reasonable spatial resolution, generating mass spectra for defined tissue pixels rapidly, while LC-MS/MS offers high-throughput, deep proteomic coverage. Such integration allows for precise annotation and localization of proteins within specific cellular populations *in situ* of the same tissue section. By doing so, it addresses the limitations of traditional methods that often lack sufficient resolution and contextual information.

Here we have utilized MALDI-IMS to quickly gain spatial information about the distribution of proteins within the brain at an almost single cell resolution. While MALDI-IMS can identify molecular heterogeneities within a given tissue, it does not allow simultaneous *in situ* identification. The assignment of IMS peptides is still a debated issue in the field and although a few approaches have attempted to resolve this, a

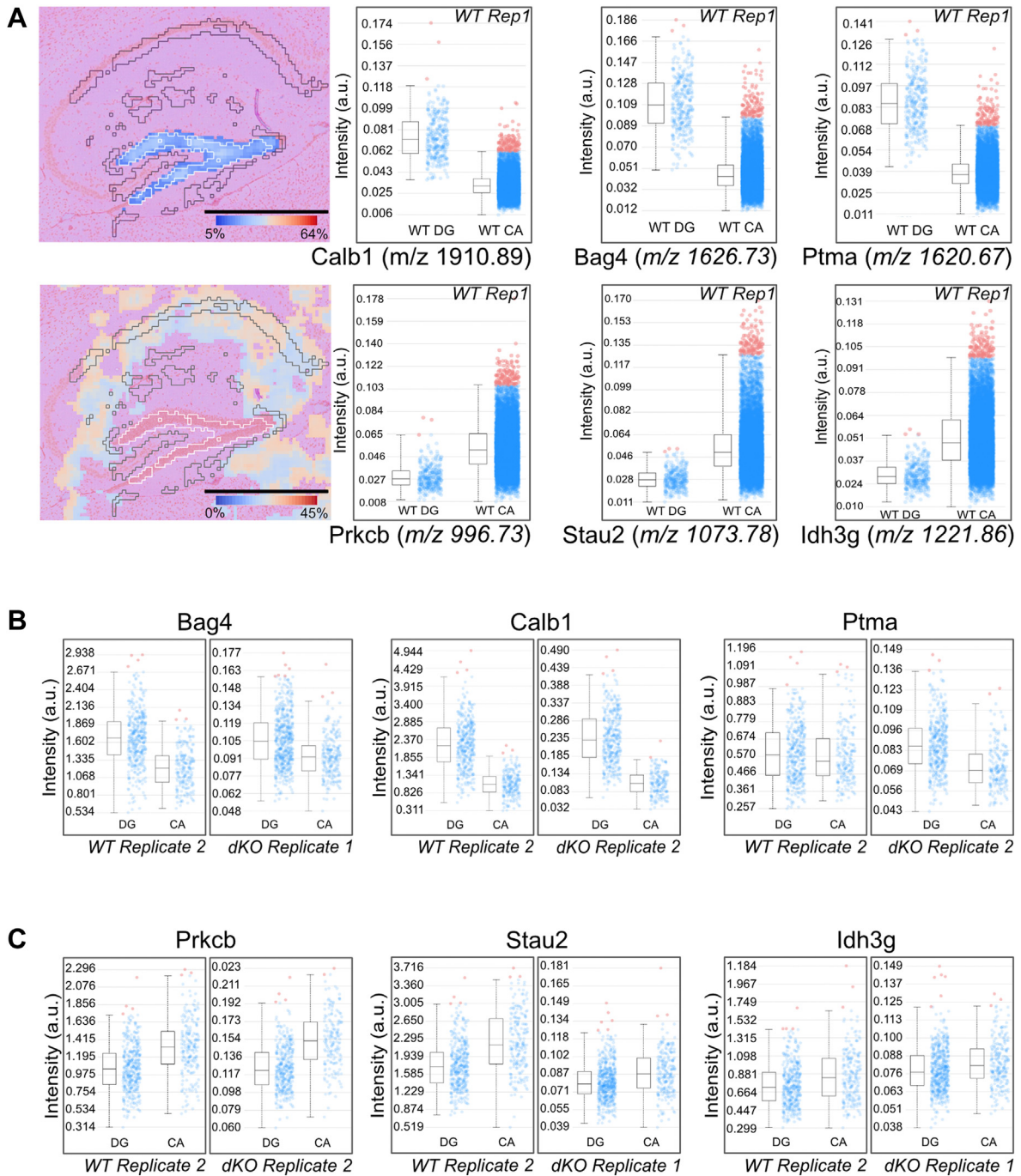


FIG. 3. Hippocampal neuronal clusters are defined by distinct proteomic signatures. *A*, representative images for peptide distributions are shown for Calb1 and Prkcb as examples of DG- and CA-discriminative proteins, respectively. Box plots showing quantification of the respective peptide signals across the measured pixels within DG (*Top panel*) and CA1 (*Bottom panel*). *B*, intensity quantifications of DG-discriminative proteins displayed in (*A*), from additional replicates. *C*, intensity quantifications of CA1-discriminative proteins displayed in (*A*), from additional replicates.

systematic, resource-independent approach with a general purpose did not exist. Using our previously developed strategy of integrating two orthogonal methods (MALDI-IMS and LC-MS/MS) allowed us to assign probable identities to multiple proteins *in situ* in a relatively short time frame compared

to other methods (14, 38, 39). Laser capture microdissection of the regions of interest enabled improvement in depth and coverage of the regional proteome, thereby eliminating potential masking effects from bulk tissue preparations. In addition, this strategy helped to expand the applicability of

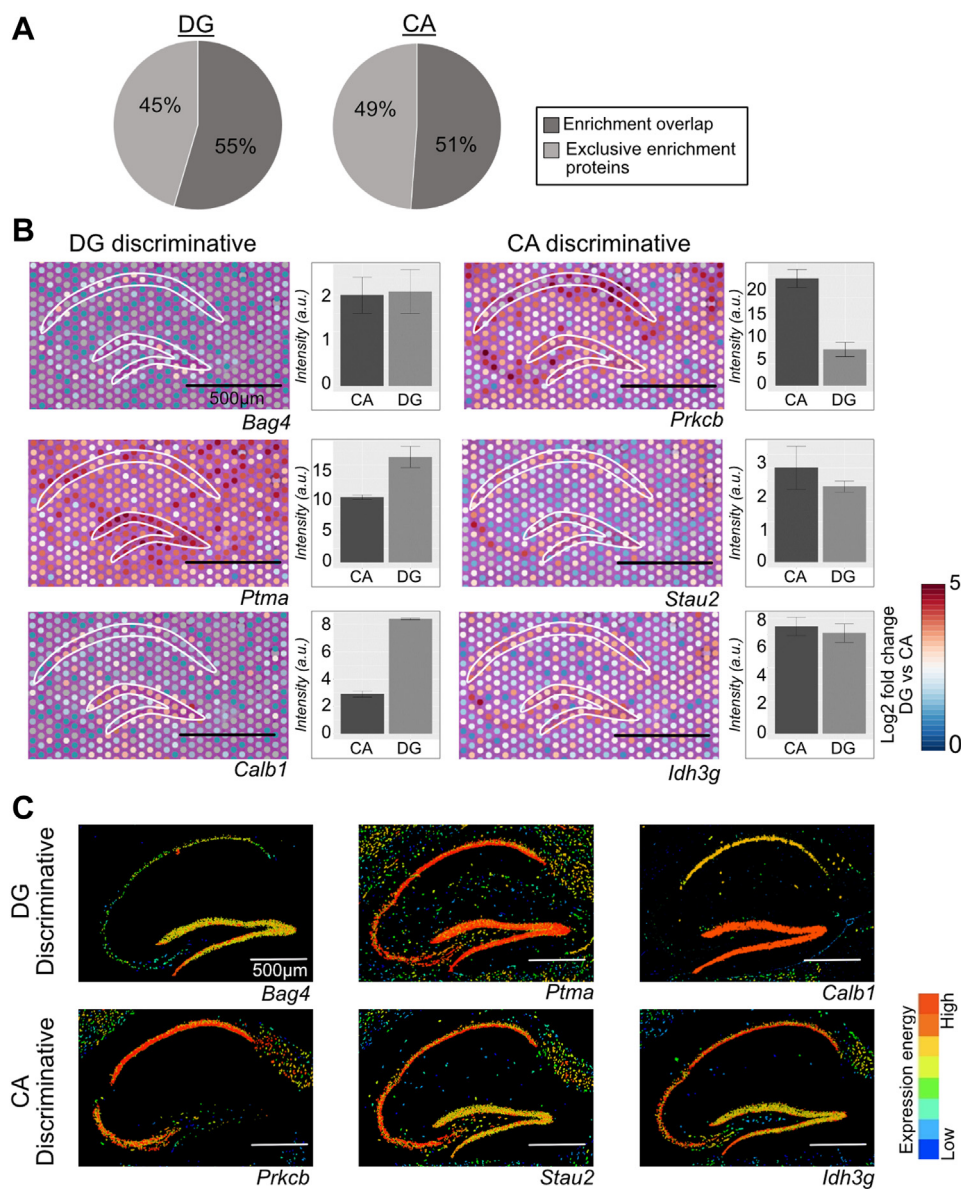


FIG. 4. Validation of spatial localization of discriminative proteins. **A**, analysis of enrichment of discriminative proteins on the transcript level. Around 55% display DG-specific enrichment on both levels, while 45% are only discriminative on the protein level (*Left pie chart*). In the case of CA1, the corresponding percentages are around 51 and 49 (*Right pie chart*). **B**, representative images of transcript distributions and intensity quantifications, corresponding to peptide quantifications shown in Fig. 3A. **C**, gene expression profiles of the above-mentioned proteins as displayed by previous research (deposited at Allen Brain Atlas) [*Bag4*: <https://mouse.brain-map.org/experiment/show/68844241>; *Ptma*: <https://mouse.brain-map.org/experiment/show/69816721>; *Calb1*: <https://mouse.brain-map.org/experiment/show/75457488>; *Prkcb*: <https://mouse.brain-map.org/experiment/show/69104118>; *Stau2*: <https://mouse.brain-map.org/experiment/show/248566>; *Idh3g*: <https://mouse.brain-map.org/experiment/show/69735216>].

ImShot in annotating peptide masses within different regions of the same tissue and different cellular subpopulations within the same region.

To demonstrate the power of this novel method, we focused on different regions of the mouse brain hippocampus. The dentate gyrus (DG), and the CA1 illustrates the importance of location-mediated neuronal connections and hence, their activity very well. We could annotate and localize proteins characteristic of several distinct regions within this brain area.

Through unbiased clustering of MALDI-IMS data, distinct peptide compositions characterizing different subpopulations were identified. Concordant with a higher nuclear density, a larger proportion of the annotated parent proteins within DG were of nuclear origin. The clustering as well as the relative abundances of corresponding parent proteins were consistent across multiple animals, and also validated through spatial transcriptomics and *in silico* approaches confirming the enrichment of identified proteins in their respective regions.

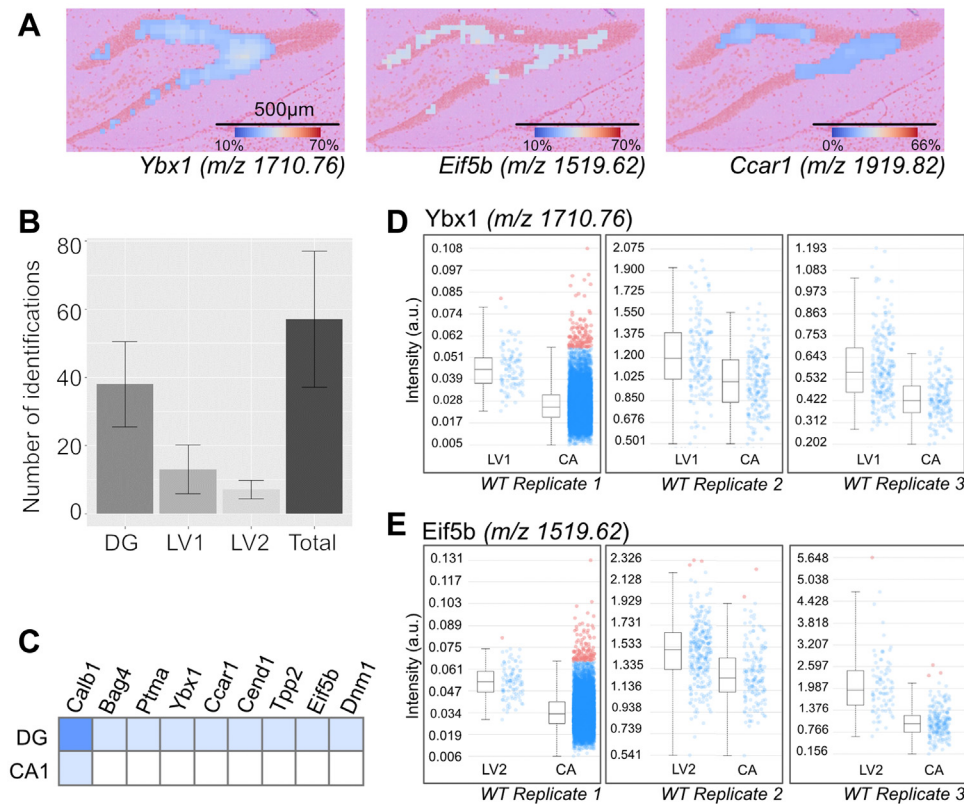


FIG. 5. Identification of local protein variations within the dentate gyrus. *A*, representative images of peptides showing the variable distribution across the granule cell layer. Scale bar = 500 μm . *B*, Number of identifications when considering DG alone, as well as proteins showing local variation with pattern 1 (LV1) or pattern 2 (LV2) and the sum of total identifications (Total). *C*, *in silico* validation of protein identification by gene expression data from MGI database. Blue = gene expression annotated as present in the structure, White = no annotation for this gene in the tissue. *D*, representative intensity quantification of Ybx1, which shows local variation with pattern 1 (LV1) and is shared across animals. *E*, representative intensity quantification of Eif5b, which shows local variation with pattern 2 (LV2) and is shared across animals.

This highlights the general applicability of our pipeline in generating reproducible and biologically relevant data.

Besides the efficient proteomic description of individual regions within a tissue, our pipeline also allowed us to detect cellular variations of proteins. We consistently observed local variations within the DG across different animals, genotypes, and areas within the tissue. The heterogeneity in the spatial distribution of distinct proteins now enables us to further investigate the nature and physiological importance of this heterogeneity.

The described pipeline represents a significant technological advancement, being less time-intensive and more cost-effective than previous methods that allow for confident assignment of protein identities at a near-single cell scale *in situ*. The pipeline demonstrates a notable improvement over existing strategies in being high-throughput, reasonably spatially resolved, platform-independent, and flexible (38, 53, 54). Measurement and data processing from an area like a mouse brain hippocampus can be done in 4 to 5 h followed by 15 min of data integration in ImShot for *in situ* protein annotation at an overall spatial resolution of 20 μm . The profiling of the hippocampus proteome at the single-cell level to uncover heterogeneity would typically require several days

to weeks using shotgun proteomics at this resolution. Our innovative approach therefore paves the way for more detailed investigations into cellular heterogeneity, with potential applications in studying disease-induced cellular changes and responses. By enabling high-throughput, spatially resolved proteomics, this technology can significantly contribute to the field of biomedical research, offering deeper insights into the molecular underpinnings of diseases such as cancer, neurological disorders, infertility, etc. Furthermore, the method's general applicability to different tissues, molecules, and biological conditions holds promise for broadening our chances to study cellular subpopulations in various contexts. Depending on the molecular analyte, the spatial resolution can further be increased *in situ*. In summary, the integration of MALDI-IMS with LCM LC-MS/MS represents a powerful tool in spatial proteomics, providing a high-resolution, high-throughput approach for studying proteomic heterogeneity within a tissue region defined by a single cell type. This methodology can be applied to identify and profile distinct molecular and cellular subpopulations, offering valuable insights into the molecular complexity of tissues.

DATA AVAILABILITY

The mass spectrometry proteomics data along with the search parameters and results files have been deposited to the ProteomeXchange Consortium via the PRIDE [1] partner repository with the dataset identifier PXD044958.

The spatial transcriptomics data has been submitted to Gene Expression Omnibus (GEO), which is available with the identifier GSE242688.

The ImShot desktop application is available at <https://github.com/wasimaftab/ImShot>

All other data used for analysis, interpretation and creation of figures are provided as Supplemental information/files with this manuscript.

Supplemental data—This article contains [supplemental data](#).

Acknowledgments—The authors thank Dr Ignasi Forne of the Protein analysis unit (ZfP) at BioMedical Center (BMC), LMU, for his help with the LC–MS measurements. Thanks are due to Dr Changjun Yin of Institute for Cardiovascular Prevention (IPEK), LMU for his immense help with training and access to the LCM instrumentation. We thank Astrid Erdmann of Bruker Daltonics GmbH for her technical support during IMS data calibration. Mouse brain samples were kindly provided from the late Dr Paolo Sassone-Corsi (University of California, Irvine).

Funding and additional information—This work was supported by grants from the Deutsche Forschungsgemeinschaft (DFG) to AI (CRC1123-TPZ02, CRC1309-TPB03, CRC1064-TPZ03). Work was supported by grants from the German Center for Diabetes Research (DZD Next 2019) and the Fritz-Thyssen Stiftung (Az.10.19.2.027MN) to R. T. Part of the work was supported by the laboratory funding of Forschungsmodul Medizin program of the Medical Faculty, LMU to S. L.

Author contributions—F. S., A. T., and S. L. data curation; F. S., A. T., and S. L. formal analysis; F. S., A. T., and S. L. investigation; F. S. and S. L. methodology; F. S. and S. L. software; F. S., A. T., and S. L. validation; F. S. and S. L. visualization; F. S. and S. L. writing—original draft; F. S., S. S., R. T., A. I., and S. L. writing—review & editing; S. S., R. T., and S. L. resources; R. T. and A. I. funding acquisition; A. I. and S. L. conceptualization, A. I. and S. L. supervision; S. L. project administration.

Conflict of interest—The authors declare that they have no conflicts of interest with the contents of this article.

Abbreviations—The abbreviations used are: CA, cornu ammonis; CA1, cornu ammonis 1; DG, dentate gyrus; GO, gene ontology; LCM, laser capture microdissection; LV1, local variation pattern 1; LV2, local variation pattern 2; MALDI-IMS, matrix-assisted laser desorption/ionization imaging mass

spectrometry; MLP, most likely peptide; ROC, receiver operating characteristic.

Received September 6, 2023, and in revised form, June 13, 2024
Published, MCPRO Papers in Press, July 11, 2024, <https://doi.org/10.1016/j.mcpro.2024.100811>

REFERENCES

- Sjöstedt, E., Fagerberg, L., Hallström, B. M., Häggmark, A., Mitsios, N., Nilsson, P., *et al.* (2015) Defining the human brain proteome using transcriptomics and antibody-based profiling with a focus on the cerebral cortex. *PLoS One* **10**, e0130028
- Hawrylycz, M. J., Lein, E. S., Guillozet-Bongaarts, A. L., Shen, E. H., Ng, L., Miller, J. A., *et al.* (2012) An anatomically comprehensive atlas of the adult human brain transcriptome. *Nature* **489**, 391–399
- Li, Q., Cheng, Z., Zhou, L., Darmanis, S., Neff, N. F., Okamoto, J., *et al.* (2019) Developmental heterogeneity of microglia and brain myeloid cells revealed by deep single-cell RNA sequencing. *Neuron* **101**, 207–223
- Molenaar, B., and van Rooij, E. (2018) Single-cell sequencing of the mammalian heart: time to dive deeper. *Circ. Res.* **123**, 1033–1035
- Doll, S., Dreßen, M., Geyer, P. E., Itzhak, D. N., Braun, C., Doppler, S. A., *et al.* (2017) Region and cell-type resolved quantitative proteomic map of the human heart. *Nat. Commun.* **8**, 1469
- Asp, M., Giacomello, S., Larsson, L., Wu, C., Fürth, D., Qian, X., *et al.* (2019) A spatiotemporal organ-wide gene expression and cell atlas of the developing human heart. *Cell* **179**, 1647–1660
- Aizarani, N., Saviano, A., Maily, L., Durand, S., Herman, J. S., Pessaux, P., *et al.* (2019) A human liver cell atlas reveals heterogeneity and epithelial progenitors. *Nature* **572**, 199–204
- Messner, C. J., Babrak, L., Titolo, G., Caj, M., Miho, E., and Suter-Dick, L. (2021) Single Cell Gene Expression analysis in a 3D microtissue liver model reveals cell type-specific responses to pro-fibrotic TGF- β 1 stimulation. *Int. J. Mol. Sci.* **22**, 4372
- Ölander, M., Wiśniewski, J. R., and Artursson, P. (2020) Cell-type-resolved proteomic analysis of the human liver. *Liver Int.* **40**, 1770–1780
- Chung, J.-J., Goldstein, L., Chen, Y.-J. J., Lee, J., Webster, J. D., Roose-Girma, M., *et al.* (2020) Single-cell transcriptome profiling of the kidney glomerulus identifies key cell types and reactions to injury. *J. Am. Soc. Nephrol.* **31**, 2341–2354
- Liao, J., Yu, Z., Chen, Y., Bao, M., Zou, C., Zhang, H., *et al.* (2020) Single-cell RNA sequencing of human kidney. *Sci. Data* **7**, 4
- Muto, Y., Wilson, P. C., Ledru, N., Wu, H., Dimke, H., Waikar, S. S., *et al.* (2021) Single cell transcriptional and chromatin accessibility profiling redefine cellular heterogeneity in the adult human kidney. *Nat. Commun.* **12**, 1–17
- Jagadeesh, K. A., Dey, K. K., Montoro, D. T., Mohan, R., Gazal, S., Engreitz, J. M., *et al.* (2022) Identifying disease-critical cell types and cellular processes by integrating single-cell RNA-sequencing and human genetics. *Nat. Genet.* **54**, 1479–1492
- Lahiri, S., Aftab, W., Walenta, L., Strauss, L., Poutanen, M., Mayerhofer, A., *et al.* (2021) MALDI-IMS combined with shotgun proteomics identify and localize new factors in male infertility. *Life Sci. Alliance* **4**, e202000672
- Anusha-Kiran, Y., Mol, P., Dey, G., Bhat, F. A., Chatterjee, O., Deolankar, S. C., *et al.* (2022) Regional heterogeneity in mitochondrial function underlies region specific vulnerability in human brain ageing: implications for neurodegeneration. *Free Radic. Biol. Med.* **193**, 34–57
- Kashima, Y., Sakamoto, Y., Kaneko, K., Seki, M., Suzuki, Y., and Suzuki, A. (2020) Single-cell sequencing techniques from individual to multiomics analyses. *Exp. Mol. Med.* **52**, 1419–1427
- Liu, J., Tran, V., Vemuri, V. N. P., Byrne, A., Borja, M., Kim, Y. J., *et al.* (2023) Concordance of MERFISH spatial transcriptomics with bulk and single-cell RNA sequencing. *Life Sci. Alliance* **6**, e202201701
- Mund, A., Brunner, A.-D., and Mann, M. (2022) Unbiased spatial proteomics with single-cell resolution in tissues. *Mol. Cell* **82**, 2335–2349
- Vandereyken, K., Sifrim, A., Thienpont, B., and Voet, T. (2023) Methods and applications for single-cell and spatial multi-omics. *Nat. Rev. Genet.* **24**, 494–515
- Zhang, D., Deng, Y., Kukanja, P., Agirre, E., Bartosovic, M., Dong, M., *et al.* (2023) Spatial epigenome–transcriptome co-profiling of mammalian tissues. *Nature* **616**, 113–122

21. Zhang, H., Liu, Y., Fields, L., Shi, X., Huang, P., Lu, H., *et al.* (2023) Single-cell lipidomics enabled by dual-polarity ionization and ion mobility-mass spectrometry imaging. *Nat. Commun.* **14**, 5185
22. Ståhl, P. L., Salmén, F., Vickovic, S., Lundmark, A., Navarro, J. F., Magnusson, J., *et al.* (2016) Visualization and analysis of gene expression in tissue sections by spatial transcriptomics. *Science* **353**, 78–82
23. Vickovic, S., Eraslan, G., Salmén, F., Klughammer, J., Stenbeck, L., Schapiro, D., *et al.* (2019) High-definition spatial transcriptomics for *in situ* tissue profiling. *Nat. Methods* **16**, 987–990
24. Taylor, M. J., Lukowski, J. K., and Anderton, C. R. (2021) Spatially resolved mass spectrometry at the single cell: recent innovations in proteomics and metabolomics. *J. Am. Soc. Mass Spectrom.* **32**, 872–894
25. Liu, J., Hu, W., Han, Y., and Nie, H. (2023) Recent advances in mass spectrometry imaging of single cells. *Anal. Bioanal. Chem.* **415**, 4093–4110
26. Lohani, V. A., Kundu, A. R. S., Akhter, M. D. Q., and Bag, S. (2023) Single-cell proteomics with spatial attributes: tools and techniques. *ACS Omega* **8**, 17499–17510
27. Mund, A., Coscia, F., Kriston, A., Hollandi, R., Kovács, F., Brunner, A.-D., *et al.* (2022) Deep Visual Proteomics defines single-cell identity and heterogeneity. *Nat. Biotechnol.* **40**, 1231–1240
28. Cornett, D. S., Reyzer, M. L., Chaurand, P., and Caprioli, R. M. (2007) MALDI imaging mass spectrometry: molecular snapshots of biochemical systems. *Nat. Methods* **4**, 828–833
29. Chen, R., Wu, X., Jiang, L., and Zhang, Y. (2017) Single-cell RNA-seq reveals hypothalamic cell diversity. *Cell Rep.* **18**, 3227–3241
30. Masuda, T., Sankowski, R., Staszewski, O., Böttcher, C., Amann, L., Scheiwe, C., *et al.* (2019) Spatial and temporal heterogeneity of mouse and human microglia at single-cell resolution. *Nature* **566**, 388–392
31. Böttcher, C., Schlickeiser, S., Sneeboer, M. A. M., Kunkel, D., Knop, A., Paza, E., *et al.* (2019) Human microglia regional heterogeneity and phenotypes determined by multiplexed single-cell mass cytometry. *Nat. Neurosci.* **22**, 78–90
32. Soltesz, I., and Losonczy, A. (2018) CA1 pyramidal cell diversity enabling parallel information processing in the hippocampus. *Nat. Neurosci.* **21**, 484–493
33. Wegrzyn, D., Juckel, G., and Faissner, A. (2022) Structural and functional deviations of the Hippocampus in schizophrenia and schizophrenia animal models. *Int. J. Mol. Sci.* **23**, 5482
34. Bartsch, T., and Wulff, P. (2015) The hippocampus in aging and disease: from plasticity to vulnerability. *Neuroscience* **309**, 1–16
35. Small, S. A., Schobel, S. A., Buxton, R. B., Witter, M. P., and Barnes, C. A. (2011) A pathophysiological framework of hippocampal dysfunction in ageing and disease. *Nat. Rev. Neurosci.* **12**, 585–601
36. Tatu, L., and Vuillier, F. (2014) Structure and vascularization of the human hippocampus. *Hippocampus Clin. Neurosci.* **34**, 18–25
37. Knowles, W. D. (1992) Normal anatomy and neurophysiology of the hippocampal formation. *J. Clin. Neurophysiol.* **9**, 253–263
38. Aftab, W., Lahiri, S., and Imhof, A. (2022) ImShot: an open-source software for probabilistic identification of proteins *in situ* and visualization of proteomics data. *Mol. Cell Proteomics* **21**, 100242
39. Huber, K., Khamehgar-Silz, P., Schramm, T., Gorshkov, V., Spengler, B., and Römpf, A. (2018) Approaching cellular resolution and reliable identification in mass spectrometry imaging of tryptic peptides. *Anal. Bioanal. Chem.* **410**, 5825–5837
40. Vitaterna, M. H., Selby, C. P., Todo, T., Niwa, H., Thompson, C., Fruechte, E. M., *et al.* (1999) Differential regulation of mammalian period genes and circadian rhythmicity by cryptochromes 1 and 2. *Proc. Natl. Acad. Sci. U. S. A.* **96**, 12114–12119
41. Deininger, S.-O., Ebert, M. P., Futterer, A., Gerhard, M., and Rocken, C. (2008) MALDI imaging combined with hierarchical clustering as a new tool for the interpretation of complex human cancers. *J. Proteome Res.* **7**, 5230–5236
42. Deutschens, F., Yang, J., and Caprioli, R. M. (2011) High spatial resolution imaging mass spectrometry and classical histology on a single tissue section. *J. Mass Spectrom.* **46**, 568–571
43. Paul, C. A., Beltz, B., and Berger-Sweeney, J. (2008) The nissl stain: a stain for cell bodies in brain sections, *CSH Protoc* 2008. *Protein Data Bank*, prot4805
44. Tyanova, S., Temu, T., and Cox, J. (2016) The MaxQuant computational platform for mass spectrometry-based shotgun proteomics. *Nat. Protoc.* **11**, 2301–2319
45. Yu, G., Wang, L.-G., Han, Y., and He, Q.-Y. (2012) clusterProfiler: an R package for comparing biological themes among gene clusters. *OMICS* **16**, 284–287
46. Lein, E. S., Hawrylycz, M. J., Ao, N., Ayres, M., Bensinger, A., Bernard, A., *et al.* (2007) Genome-wide atlas of gene expression in the adult mouse brain. *Nature* **445**, 168–176
47. Allen Institute for Brain Science. (2004) Allen mMouse bBrain aAtlas [68844241]. Available from: mouse.brain-map.org
48. Allen Institute for Brain Science. (2004) Allen mMouse bBrain aAtlas [69816721]. Available from: mouse.brain-map.org
49. Allen Institute for Brain Science. (2004) Allen mMouse bBrain aAtlas [75457488]. Available from: mouse.brain-map.org
50. Allen Institute for Brain Science. (2004) Allen mMouse bBrain aAtlas [69104118]. Available from: mouse.brain-map.org
51. Allen Institute for Brain Science. (2004) Allen mMouse bBrain aAtlas [248566]. Available from: mouse.brain-map.org
52. Allen Institute for Brain Science. (2004) Allen mMouse bBrain aAtlas [69735216]. Available from: mouse.brain-map.org
53. [preprint] Ryu, T., Kim, S.-Y., Thuraisamy, T., Jang, Y., and Na, C. H. (2023) Development of an *in situ* cell-type specific proteome analysis method using antibody-mediated biotinylation. *bioRxiv*. <https://doi.org/10.1101/2023.06.13.544682>
54. Oliveira, C., and Longuespée, R. (2023) MALDImlD: spatialomics R package and Shiny app for more specific identification of MALDI imaging proteolytic peaks using LC-MS/MS-based proteomic biomarker discovery data. *Proteomics* **23**, e2300005